Current Measurement by Use of Synchronous Wave probes: Method and Example of Laboratory experiments for Progressive or Partially Standing Waves

A. Cuevas, V. Rey, Fabrice Ardhuin, Julien Touboul

Current Measurement by Use of Synchronous Wave probes: Method and Example of Laboratory experiments for Progressive or Partially Standing Waves

A. Cuevas[a], V. Rey[a,*], F. Ardhuin[b] and J. Touboul[c]

[a]Université de Toulon, Aix-Marseille Université, CNRS/INSU, Mediterranean Institute of Oceanography (MIO), UM AMU 110, Toulon Cedex, 83041, France

[b]LOPS, Université de Bretagne Occidentale; CNRS; Ifremer; IRD, Technopôle Brest Iroise, Plouzané, 29280, France

[c]Ecole Centrale de Marseille, Aix Marseille Université, CNRS, IRPHE UMR 7342, Marseille, 13384, France

ARTICLE INFO

Keywords:
Waves
Currents
Progressive waves
Partially standing waves
Vertically sheared currents
Laboratory data analysis

ABSTRACT

In the context of studies of interactions between waves and currents, a method of calculation of the current through synchronous free surface deformation measurements at various locations is proposed and discussed in the case of either progressive or partially standing waves, and for either homogeneous or vertically sheared current. For partially standing waves, the method takes advantage of separation of incident and reflected wave method through minimisation algorithms, which are still applicable in the limit case of a progressive wave. Discussions on the accuracy of the method are based on comparisons to laboratory experiments including regular and irregular waves in following or opposite current conditions. The vertically averaged current is recovered since current has a significant influence on the wave celerity. Vertically shear has less influence on the wave celerity in comparison to the averaged current in the experimental conditions considered, and is hardly directly recovered because of the noise inherent to the measurements. However the shear can be estimated through the calculated vertically averaged current which depends on frequency in the presence of shear. The present study concerns the unidirectional case, including regular or irregular waves.

1. Introduction

Wave conditions from open sea to coast provide necessary information for understanding coastal dynamics, designing engineering structures, navigation and assessing flooding risks. They are also a potential means of accessing information present beneath the surface, such as bathymetry or currents. The reflection, refraction and diffraction of waves are forced not only by changes in bathymetry but also by the presence of currents. Traditional numerical models were limited to homogeneous currents in the water column, thus preserving the irrotational nature of wave-induced flow. However, vertically sheared currents are frequently observed, because of the wind, tides, or waves (Soulsby, 1990; Haas and Svendsen, 2002). Some decades ago, the impact of a vertically sheared current on wave propagation speed was explored (Kirby and Chen, 1989). Additionally, these shears can arise or be intensified due to sudden changes in bathymetry (Rey et al., 2014). Recent models have emerged to depict the propagation of regular waves in vertically sheared current, initially considering constant shear (Touboul et al., 2016) and later accommodating arbitrary shear profiles (Touboul and Belibassakis, 2019). These models were then extended to address scenarios with waves strongly reflected by a sinusoidal seabed (Belibassakis et al., 2019; Laffitte et al., 2021). The coexistence of a current collinear with the wave alters its propagation speed. For years this Doppler effect has been employed to measure surface currents through HF Radar measurements (Stewart and Joy, 1974). It is used to calculate the speed of the surface current averaged over a thickness that depends on the wavelength of the surface wave component which corresponds to the half-wavelength of the radar, the measurement principle being based on Bragg resonance for electromagnetic wave scattering, and the shift of the resonant Doppler peak due to the current component in the electromagnetic wave direction. Signal coherence is the key to determining the phase shift, as done for instance to establish wave speed and implicitly current speed through remote sensing (Yurovskaya et al., 2019). Since vertically sheared currents affect the celerity of progressive waves differently according to their frequency, methods for reconstructing current profiles from

*Corresponding author
rey@univ-tln.fr (V. Rey)
ORCID(s):

spectral wave data have been proposed by Smeltzer et al. (2019). However, in the case of partially standing waves, wave phase evolves differently along the incoming wave direction. Due to bathymetric changes or engineering structures, reflection may occur. Even far from the coast, waves of opposing directions also exist, as for instance demonstrated by Bragg resonant peaks for both directions through HF Radar measurements. For known current conditions, separation algorithm derived from classical least square method (Mansard and Funke, 1980) were proposed for homogeneous current (Rey et al., 2002; Magne et al., 2005) or for constant vertical current shear (Laffitte et al., 2021). This method of minimisation, which requires an oversampled system of wave gauges, allows the analytical calculation of both the complex incident and reflected wave components. In order to recover the current condition, Draycott et al. (2018, 2019) have used a frequency domain solver to resolve two opposing wave system propagating on a collinear uniform current. The method is based on a minimisation of the difference between the (assumed) theoretical wave signal and surface deformation measurements at wave gauges locations. The method then assumes a number and arrangement of probes such that the system is oversampled. They improved the optimisation process in Draycott et al. (2019) by an analytical calculation of the exact gradients of both wave amplitudes and wavenumbers instead of numerical differentiation for each frequency component. Their model was compared to experimental data carried out in the large scale FlowWave tank for various current intensities and wave spectra. The averaged mean currents were recovered by averaging the current calculated for each of the frequency components, with a weighting corresponding to the incident amplitude of the frequencies composing the wave spectrum after Fast Fourier Transform (FFT) of the free surface time series in the absence of current. They observed that turbulence may alter the quality of the results, especially for opposing wave-current conditions. Application of such a method of minimisation was then used to extract the current intensity from buoy data for wave spectra with angular distribution (Pillai et al., 2021). The present study aims to extract ocean current information including its vertical shear through analysis of synchronous wave data from wave probes. The proposed method takes advantage of the analytic expressions of both incident and reflected wave in the minimisation process (Laffitte et al., 2021). It is then intended to recover not only the vertically averaged current but also its vertical shear. In addition, the analytic expression of the complex wave in the particular case of a progressive wave is derived in order to quantify the effect of a reflected wave on the computed current. In the following, the method of minimisation is presented and applied to known progressive or partially standing monochromatic or spectral waves. The capability of the method to recover the current properties is then discussed through analysis of synchronous surface deformation data from former laboratory experiments on partially waves in following (Magne et al., 2005) or opposite current conditions (Laffitte et al., 2021).

2. Minimization method and test on perfect signals

2.1. Presentation of the method for reconstructing current fields

2.1.1. Wave properties and conditions of minimization (2D case)

In the convention frame, waves propagates along the x-axis. z-axis is vertical upwards, $z = 0$ corresponds to the still water level. The surface elevation $\eta(x,t)$ for a wave (or wave component) of frequency $f = \omega/2\pi$ resulting from two plane waves travelling in opposite directions along the x-axis is as follow

$$\eta(x,t) = a_i e^{i(\omega t - k^- x)} + a_r e^{i(\omega t + k^+ x + \phi)} \tag{1}$$

where a_i and a_r are complex amplitudes and ϕ the phase lag at origin. $k^\pm$ are the wavenumbers of the reversed and incident running waves, they are given by:

$$\sigma^\pm = (\omega \pm |U|k^\pm)^2 = gk^\pm tanh(k^\pm h) \tag{2}$$

where h is the water depth and $\sigma^\pm$ are the relative frequencies in a coordinate system travelling at velocity U. For currents with a linear vertical shear of the form $U(z) = U_0 + Sz$ the waves numbers $k^\pm$ are given by (Touboul et al., 2016):

$$(\omega \pm |U_0|k^\pm)(\omega \pm |U_2^\pm|k^\pm) = gk^\pm tanh(k^\pm h) \tag{3}$$

where $U_2^\pm$ depends on the wave frequency

$$U_2^\pm = U_0 - S\frac{tanh(k^\pm h)}{k^\pm} \tag{4}$$

The theoretical expression, based on Airy waves, for the free surface at the position x_n of probe S_n (where x_1 is the position of the first probe S_1) is given for an arbitrary choice of time zero by:

$$\eta_n = \left\{ a_i e^{-i(k^- x_1 + \Delta_n^-)} + a_r e^{+i(k^+ x_1 + \Delta_n^+ + \phi)} \right\} e^{i\omega t} \tag{5}$$

with $\Delta_n^- = k^-(x_n - x_1)$ and $\Delta_n^+ = k^+(x_n - x_1)$. The component of frequency f of the elevation of the free surface, as measured by probe S_n, with $n = 1, 2, 3...N$, is the of form

$$\eta_n^{(m)} = A_n e^{i(\omega t - \phi_n)} \tag{6}$$

where the superscript (m) indicates the measured values. The amplitude and phase A_n and ϕ_n are determined from a Fourier analysis (Fast Fourier Transform FFT)) of the signal measured by probes S_n. For $n \geq 3$ the unknown amplitudes a_i and a_r are calculated through the minimization of the error E

$$E^2 = \sum_{n=1}^{N} \left[a_i e^{-i\Delta_n^-} + a_r e^{i\Delta_n^+} - (A_n e^{i\phi_n}) \right]^2 \tag{7}$$

with respect to a_i and a_r: $\frac{\partial E^2}{\partial a_i} = \frac{\partial E^2}{\partial a_r} = 0$ (Rey et al., 2002). Theoretically, under the framework of the linear theory (Airy waves), the error must be zero in the absence of noise and error in the location of the probes. For a wave or wave component of frequency f, the right current U for homogeneous case is found for $E = 0$. For a vertically sheared current, the right current characteristics (U, S) are also found for $E = 0$ since at a given couple (U, S) corresponds a single couple (k^-, k^+). The incident and reflected wave components a_i and a_r are given by (Rey et al., 2002):

$$|a_i| = \left| \frac{s_2 s_3 - s_{12} s_4}{s_5} \right| \quad ; |a_r| = \left| \frac{s_1 s_4 - s_{12} s_3}{s_5} \right| \tag{8}$$

with

$$s_1 = \sum_{n=1}^{N} e^{-2i\Delta_n^-}; \quad s_2 = \sum_{n=1}^{N} e^{+2i\Delta_n^+}; \quad s_{12} = \sum_{n=1}^{N} e^{+i(\Delta_n^+ - \Delta_n^-)}; \tag{9}$$

$$s_3 = \sum_{n=1}^{N} A_n e^{-i(\Delta_n^- + \phi_n)}; \quad s_4 = \sum_{n=1}^{N} A_n e^{+i(\Delta_n^+ + \phi_n)}; \quad s_5 = s_1 s_2 - s_{12}^2 \tag{10}$$

For progressive wave, amplitude $a_i = a_{prog}$ and Eq 7 becomes:

$$E^2_{progressive} = \sum_{n=1}^{N} \left[a_{prog} e^{-i\Delta_n^-} - (A_n e^{i\phi_n}) \right]^2 \tag{11}$$

and the incident wave amplitude modulus:

$$a_{prog} = \left| \frac{s_3}{s_1} \right| \tag{12}$$

Since the error is proportional to the amplitude, we can normalise it by the incident amplitude a_i. Let us note that for the case of vertically sheared current, at given wavenumber k^- corresponds an infinity of couples (U, S). Calculation of (U, S) then necessitates data from at least two wave frequencies. For irregular waves, the above method is applied to each of the frequencies of the discrete wave amplitude spectrum obtained by Fast Fourier Transform of the time series. Continuous spectra can then be estimated by either frequency or amplitude averaging (Drevard et al., 2009). The same averaging process is conducted for the estimation of the current.

2.1.2. Algorithm implementation

The Fig.1 provides the step-by-step algorithms to reconstruct the current thanks to the minimization method. We choose the example of a regular progressive wave propagating in the presence of a homogeneous current $U = 0.3$ m.s^{-1}. The Fig. 1 (a) shows a section of the time series measured by the probe S_n considered in this example, where the subscript n corresponds to the number of the probe. In the following, the time series were generated to apply the method to theoretical signals, or real time series were used to apply the method to data from laboratory experiments. We then applied the Fast Fourier Transform (FFT) to this signal taking care to select a signal that gives good frequency resolution. For a regular wave, of frequency f, the time series was a multiple of the wave period $T = \frac{1}{f}$ in order to include f in the frequency values after FFT. The spectrum resulting from the FFT is shown in Fig. 1 (b). The FFT allows us to determine the amplitude A_n and the phase ϕ_n at the wave frequency, or for each frequency component for a spectral wave. We then calculate the errors E and $E_{progressive}$ using the Eq. (7) and (11) respectively. Numerically, to determine the effective value of the current, the error is evaluated by looping through the different current intensities. The evolution of the errors normalized by the amplitude as a function of current is shown in Fig. 1 (c). In this example the wave is progressive so both errors are minimal and equal 0 for the effective value of current intensity $U = 0.3$ m.s^{-1}. As already mentioned, in the case of irregular waves, these algorithms are applied to each frequency component of the discrete wave amplitude spectrum. Finally in the case of waves propagating in the presence of a current with a linear vertical profile, there are two ways of applying the method. We can either directly minimize the errors in relation to the surface current and shear with loops on both current and shear or applying in a first stage the method for a homogeneous current, and extracting the shear coefficient in a second stage by fit of the dependency of the current U versus frequency. Examples of results for known generated signals are given in the subsection 2.2.

2.2. Application on theoretical signals

2.2.1. Progressive or partially standing waves for homogeneous current

To test the above methods, time series of 200 periods are generated for either a progressive wave or a partially standing wave. We consider the case of regular waves at the water depth $h = 1.9$ m at frequencies $f_1 = 0.71$ Hz (deep water), $f_2 = 0.56$ Hz (finite depth) and $f_3 = 0.21$ Hz (shallow water). We studied the case without current and the case with a uniform current with an intensity of $U = 0.3$ m.s^{-1} and it follows the incoming wave direction. Virtual probes are displayed at locations $x = 0, 0.2, 0.5$ m. The reflection coefficient is either $R = 0\%$ or $R = 30\%$. The Tab. 1 lists all the characteristics used.

Table 1
Parameters used for the theoretical monochromatic waves

Parameters	Reg1	Reg2	Reg3	Reg4
Water depth h (m)	1.9	1.9	1.9	1.9
Frequency range (Hz)	[0.21; 0.56; 0.71]	[0.21; 0.56; 0.71]	[0.21; 0.56; 0.71]	[0.21; 0.56, 0.71]
Duration range (s)	[940; 360; 280]	[940; 360; 280]	[940; 360; 280]	[940; 360; 280]
Current intensity U (m.s^{-1})	0	0.3	0	0.3
Reflection coefficient R	0 %	0 %	30 %	30 %

As expected considering the algorithm for a partially standing wave, the right current intensity and reflection coefficients are recovered for both reflection conditions (see Fig. 2 and Fig. 3). The evolution of the error for the lowest frequency is less sensitive to the current. The minimum is less pronounced at low frequencies because at these frequencies the speed of propagation is less affected by a given current. For the algorithm that assumes a progressive wave, the effective current is recovered for the case without reflection. In the presence of reflection even quite small the error is never zero and its minimum does no longer correspond to the true current. This is due to the modification of the phase evolution along the x-axis in the presence if the reflected wave. In the case of limiting case of standing wave, the phase does no more evolve along the x-axis. However in the case of a progressive wave, the variation of the error E with respect to U is more rapid for the algorithm based on the progressive wave in the vicinity of the minimum than when using the algorithm for a partially standing wave. It is mainly due to the fact that the phase along a given path along the x-axis is more sensitive to the current than the phase lag after a return path (Rey et al., 2002). As a consequence, the method based on a partially standing wave may be more sensitive to the noise.

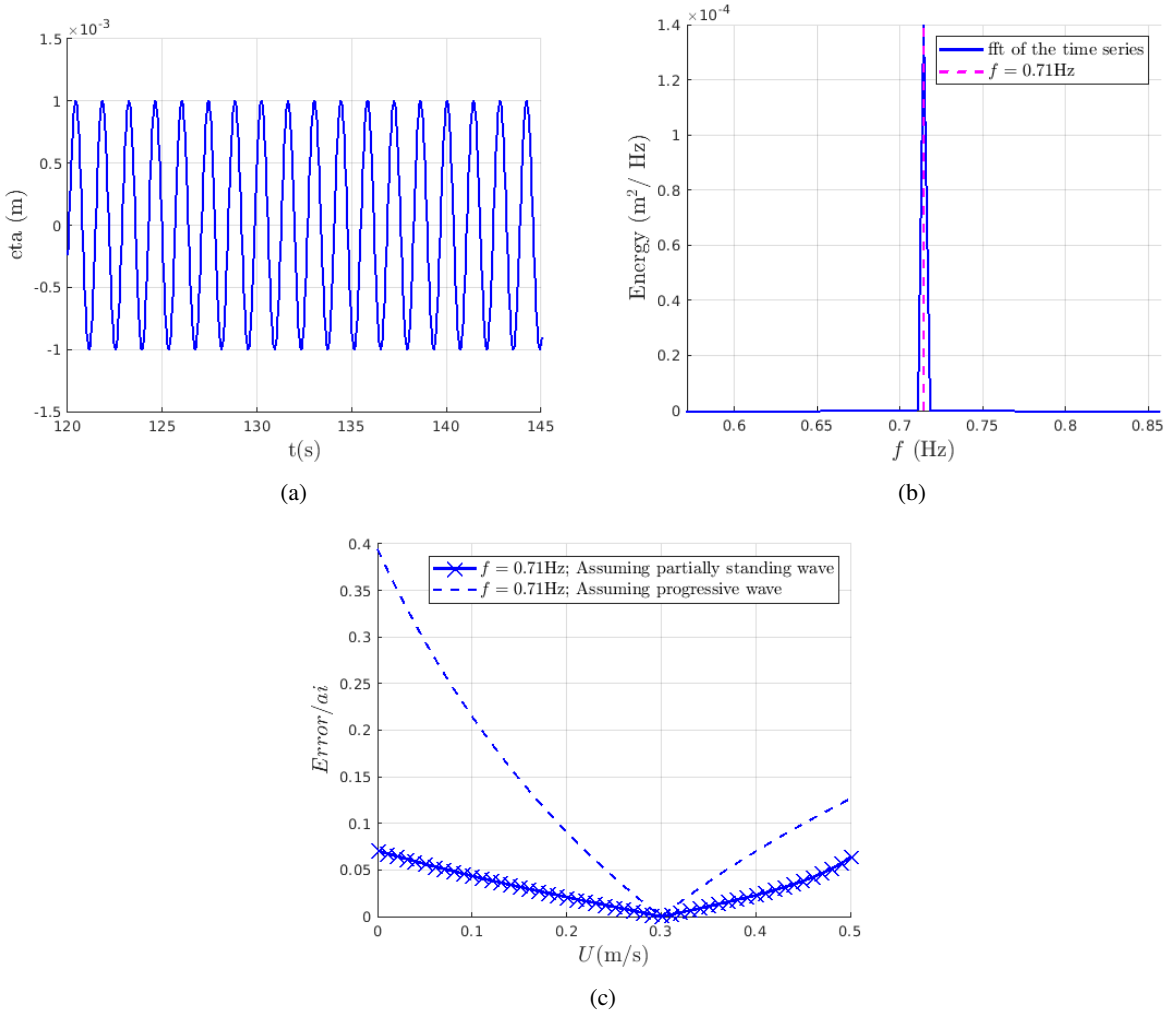

Figure 1: Numerical process for using the method of minimization. (a) time series; (b) Spectrum obtained through the FFT; (c) Evolution of errors according to the current intensity, (- -) Assuming partially standing wave and (-x-) Assuming a progressive wave

A second set of times series tested in the same water depth, current and probe's location conditions was carried out with irregular waves. Irregular waves of JONSWAP spectrum shape ($\gamma = 3.3$) with $T_p = 1.813$ s and $H = 0.12$ m (Fig. 4) are generated to create the time series. Duration of the time series was chosen to accurately represent real waves (Tabeshpour and Belvasi, 2023).

As above, we consider both cases without current and with a current intensity $U = 0.3$ m.s^{-1}. One signal includes a 30 % reflection while the second has none. The Tab. 2 lists all the characteristics used in those cases. The algorithms are then applied to each frequency component of the FFT under the assumptions of progressive and partially standing waves to determine current intensity. The current U corresponding to the minimization of E and $E_{progressive}$ is represented in Fig. 5. We observe that with the algorithm considering the reflection, the minimum error is reached for the correct theoretical value of current intensity either for the signal in the presence of current or in the absence of current. Numerical errors may explain the discrepancies at the low frequency range, since the impact of the current on the wavenumbers is weaker. At high frequency, the wave celerity against current tends to diminish (or vanish). Due to this diminishing, divergence of the coefficient s_5 may be observed.

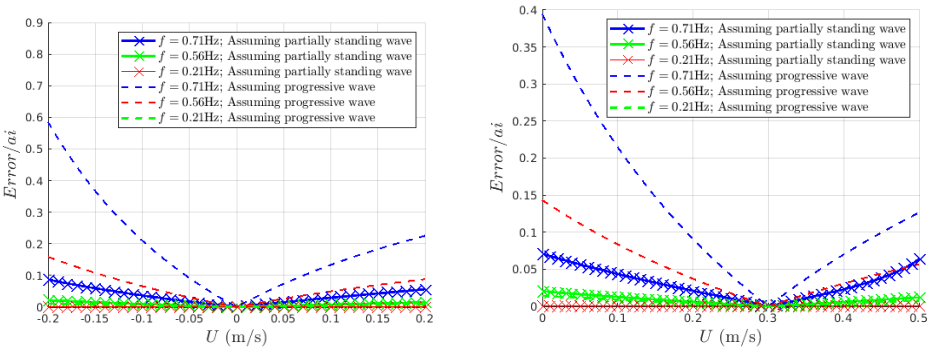

(a) Case Reg1 (b) Case Reg2

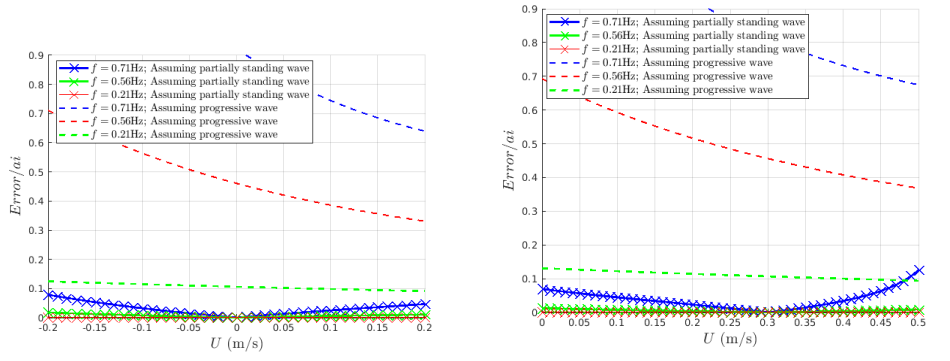

(c) Case Reg3 (d) Case Reg4

Figure 2: Normalized errors versus the current for theoretical signals. (a) Without current and $R = 0\%$ (b) $U = 0.3$ m.s^{-1} and $R = 0$ % (c) Without current and $R = 30$ % (d) $U = 0.3$ m.s^{-1} and $R = 30$ %

Table 2
Parameters used for the theoretical irregular waves

Parameters	IR1	IR2
Water depth h (m)	1.9	1.9
Peak period T_p (s)	1.813	1.813
Duration (s)	543.9	543.9
Significant wave height H_s (m)	0.12	0.12
Gamma γ	3.3	3.3
Current intensity U (m.s^{-1})	0	0.3
Reflection coefficient R	[0 %, 30 %]	[0 %, 30 %]

2.2.2. Partially standing waves for linearly sheared current

In this section the methods are tested for a partially standing wave with a linear vertically sheared current. In that case regular waves in the frequency range $0.15-1.45$ Hz with a duration of 200 periods are considered. The water depth $h = 1.9$ m, the current parameters are $U_0 = 0.3$ m.s^{-1}, $S = 0.1$ s^{-1} and the current follows the incoming wave direction. The probe's locations are the same than in, the previous part and the reflection coefficient is $R = 30$ %. The conditions used are summarised in the Tab. 3. Within the context of waves propagating in the presence of a vertically sheared current, many studies intended to establish an analogy with the case of waves propagating over a uniform current (U_{eq})). Defining the equivalent current, crucial for accurate water wave dynamics representation involves considering an equivalent depth $d_e = tanh(k^{\pm}h)/2k^{\pm}$ which tends to $\lambda^{\pm}/4\pi$ for deep water conditions (Stewart and Joy, 1974). The equivalent current is therefore $U_1 = U(z = -d_e) = U_0 - d_e S$ (Touboul et al., 2016). The method, first applied under the assumption of a uniform current yields the estimated current at depth d_e (Fig. 6). For this configuration,

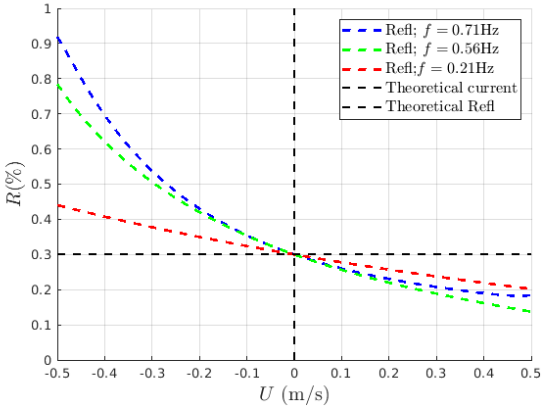

(a) Case Reg3

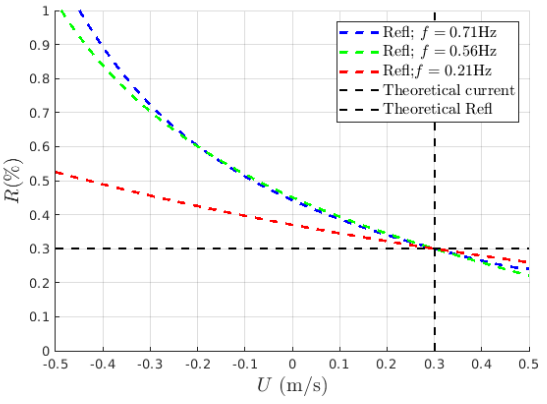

(b) Case Reg4

Figure 3: Reflection coefficient versus the current for three theoretical signals in presence of 30% of reflection (a) without current and (b) Current intensity = 0.3 m.s^{-1}

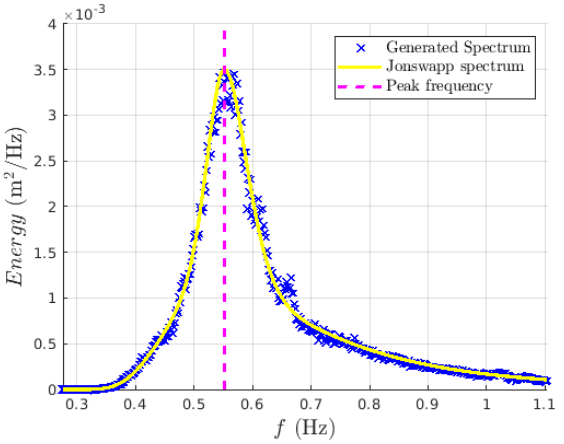

Figure 4: Jonswap and generated spectrum of the incident wave, $f_p = 0.55$ Hz

Table 3
Parameters used for the theoretical regular waves in the presence of a vertical sheared current

Parameters	Regs sheared
Water depth h (m)	1.9
Range of frequency (Hz)	[0.15 – 1.45]
Duration (s)	[96 – 800]
Surface current U_0 (m.s^{-1})	0.3
Shear parameter S (s^{-1})	0.1
Reflection coefficient R	0 %, 10 %, 30 %

maximum at the free surface, the average current seen by a wave at a given frequency is all greater the high frequency. For a current calculation based on a homogeneous current in the water column, a frequency dependent intensity could therefore mean the presence of a sheared current. Some points fall outside the expected range due to the tendency of the ratio s_5 (Eq. 11) to approach zero. As expected the algorithm considering progressive wave does not provide

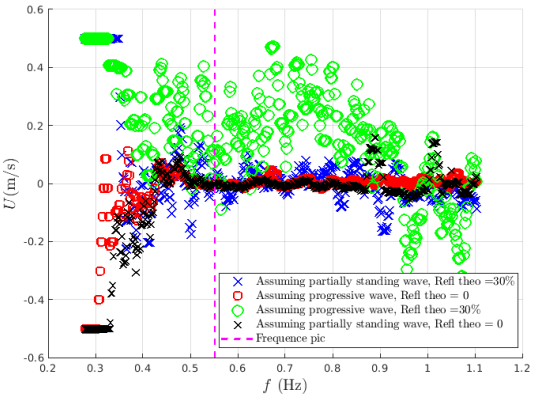

(a) Case IR1

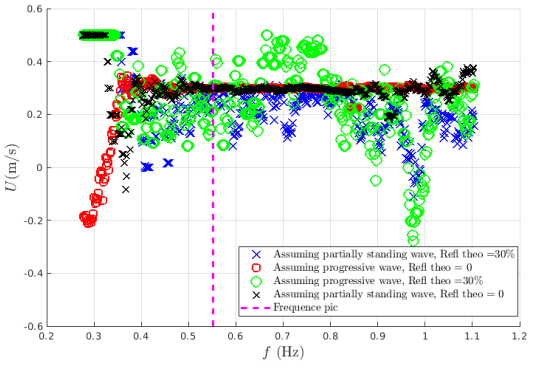

(b) Case IR2

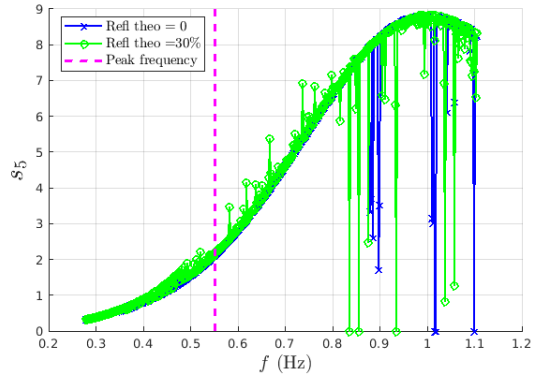

(c) Case IR1

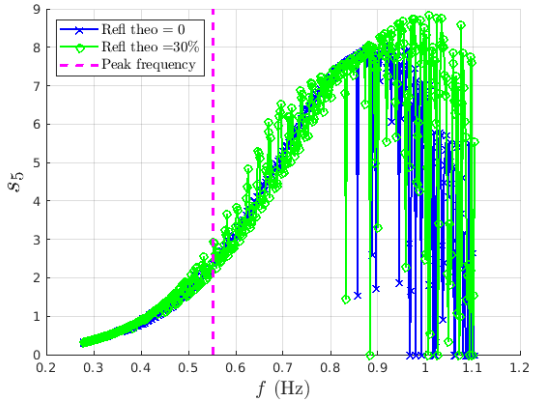

(d) Case IR2

Figure 5: Current intensity (a) signals in absence of current (b) signals with a current intensity $U = 0.3$ m.s^{-1}. Ratio s5 (c) signals in absence of current (d) signals with a current intensity $U = 0.3$ m.s^{-1}

consistent results (Fig. 6 (a)). The figure Fig. 6 (b) shows the result for different reflection coefficient and for currents $U_1(f)$ at the depth d_e which is estimated by both k^- and k^+. It focuses on the points inside the expected range and on the algorithm assuming partially standing waves. For a progressive wave ($R = 0\%$), the values found follow the current at the depth $d_e(k^-)$. For a weak reflection ($R = 10$ %) there are a few discrepancies with $U_1^-(d_e(k^-))$, but they are still in good agreement. If the reflection is stronger, we can see that at very low frequencies the current found follows $U_1^-(d_e(k^-))$, but at higher frequencies it tends towards $U_1^+(d_e(k^+))$. This means that if the reflection is significant, both depths $d_e(k^-)$ and $(d_e(k^+)$ must be taken into account the "integrated" current is then a combination of U_1^+ ans U_1^-. We can also use the algorithms under the assumption of a linear vertical sheared current and represent the evolution of E and $E_{progressive}$ with respect to both the surface current and the shear. The method is applied to two theoretical regular waves of the same frequency $f = 0.5$ Hz, one with no reflection and the other with 30 % reflection, under the same water depth and current conditions as above. Fig. 7 shows the evolution of the normalized errors in the case without reflection and the figure Fig.8 shows the result for the other case.

In the case of a progressive wave (Fig. 7) we observe that the minimum is not clearly defined, whether using the algorithm assuming progressive wave or the one assuming partially standing wave. As already mentioned, it is mainly due to the fact that for a vertically sheared current, at a given wavenumber k corresponds an infinity of couples (U_0, S). While shear minimally influences error in contrast to surface current, the error E is zero for the right couple (U_0, S). This is highlighted by Fig. 8 with the study of a regular wave in the presence of reflection. While the algorithm assuming progressive wave didn't give consistent results as expected, using the method assuming partially standing wave gave a minimum well located. Indeed, unlike the progressive case, for a given couple (k^-, k^+) corresponds a single couple

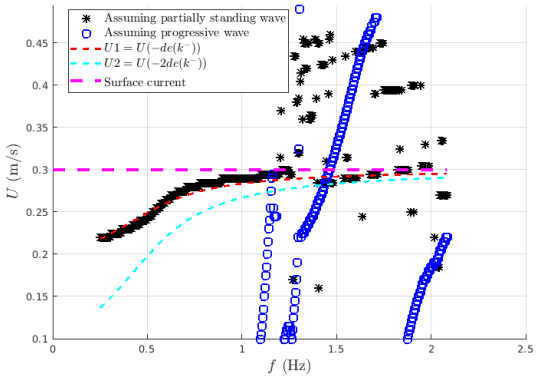

(a) Current estimated; theoretical signals; $R = 30\%$ (Partially standing waves (*); Progressive waves (**o**)

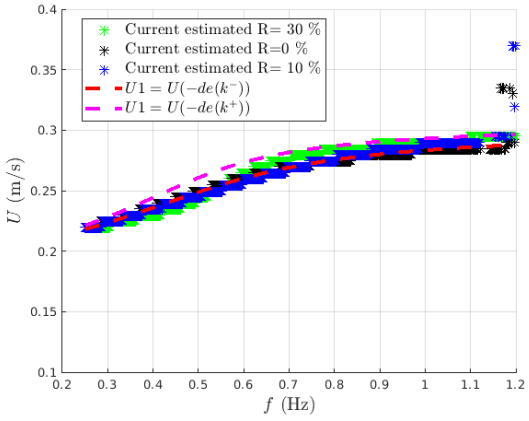

(b) Current estimated theoretical signals: Without reflection (*); $R = 10$ % (*); $R = 30$ % (*)

Figure 6: Current estimated for each regular waves

(U_0, S). Even though the error E depends much less on shear than on current, it is zero for the correct value of the couple (U_0, S).

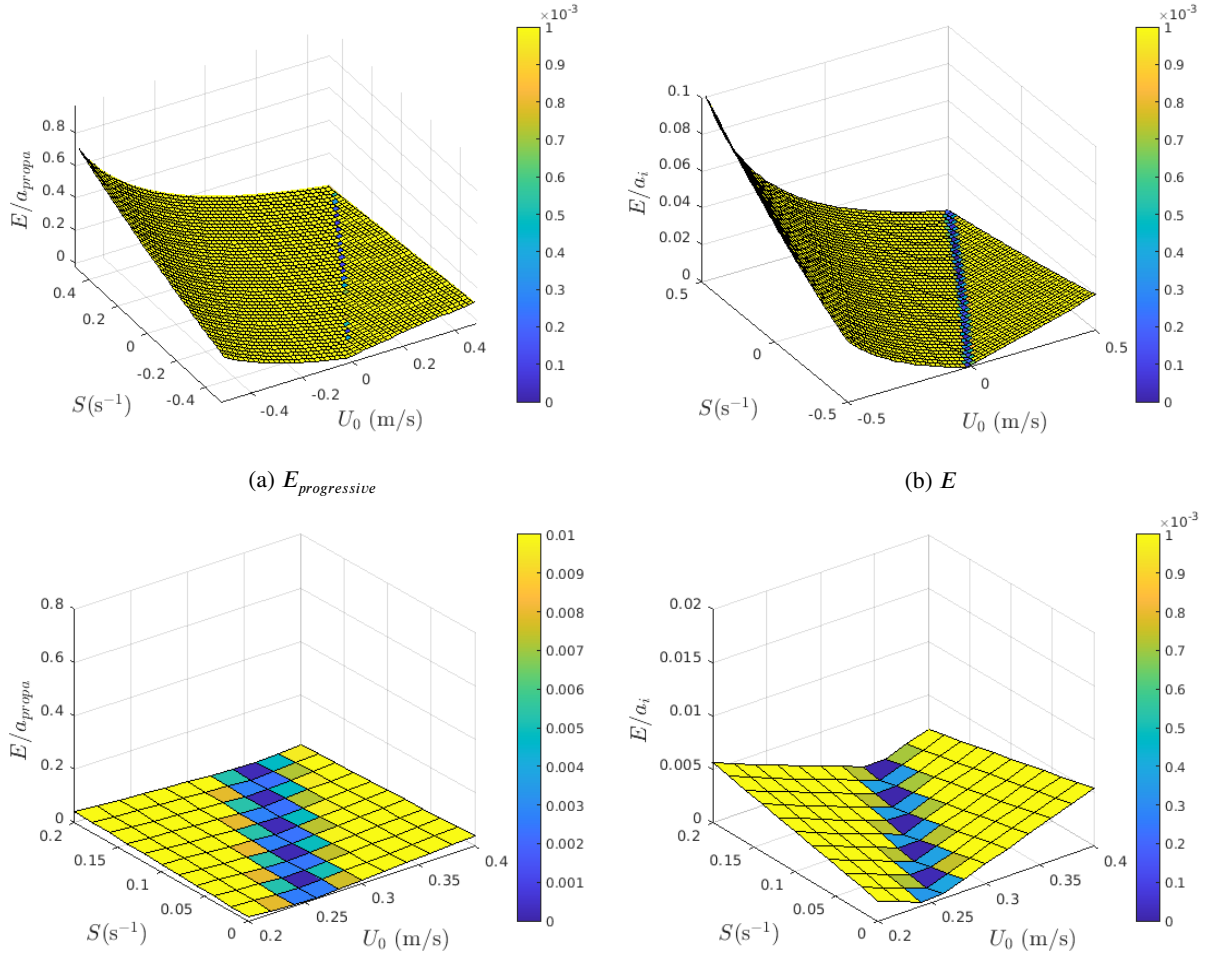

(a) $E_{progressive}$ (b) E

(c) $E_{progressive}$ zoom (d) E zoom

Figure 7: Evolution of normalized Errors for a theoretical regular wave without reflection $R = 0$ %

3. Comparison with experimental data

In this study we examined two experiments: the first outlined in Magne et al. (2005), conducted at the Ocean Engineering Basin (BGO) FIRST which is managed by the company Oceanide in la Seyne-sur-mer, France. This campaign involved regular and irregular waves in presence of a collinear uniform current. The second was carried out at the engineering school SeaTech in Toulon, France. It involved regular waves and an opposite sheared current. The detailed set-up is presented in Laffitte et al. (2021).

3.1. Monochromatic waves

3.1.1. Co-current

In this subsection we focus on the propagation of monochromatic waves in the presence of a collinear uniform current. We used the dataset from the experiment in the BGO FIRST. The BGO-FIRST is a large scale basin. It has a useful length of 24 m and an effective width of 16 m. The maximum water depth is 5 m, with a central pit of 10 m water depth that was not used in this study. It is equipped with a current generator, a wavemaker over the entire width and an X-Y carriage, working in a Cartesian coordinate system. The experimental setup is represented in Fig. 9. Initially, the goal of this campaign was the measurement of wave scattering by topography is presence of currents. The method of minimization is applied using the first four probes G1, G2, G3, G4 at the locations $x = 0, 1.45, 2.25, 2.7$ m respectively. The probes are located just right before the ramp and the sinusoidal bed, at this place the water depth is

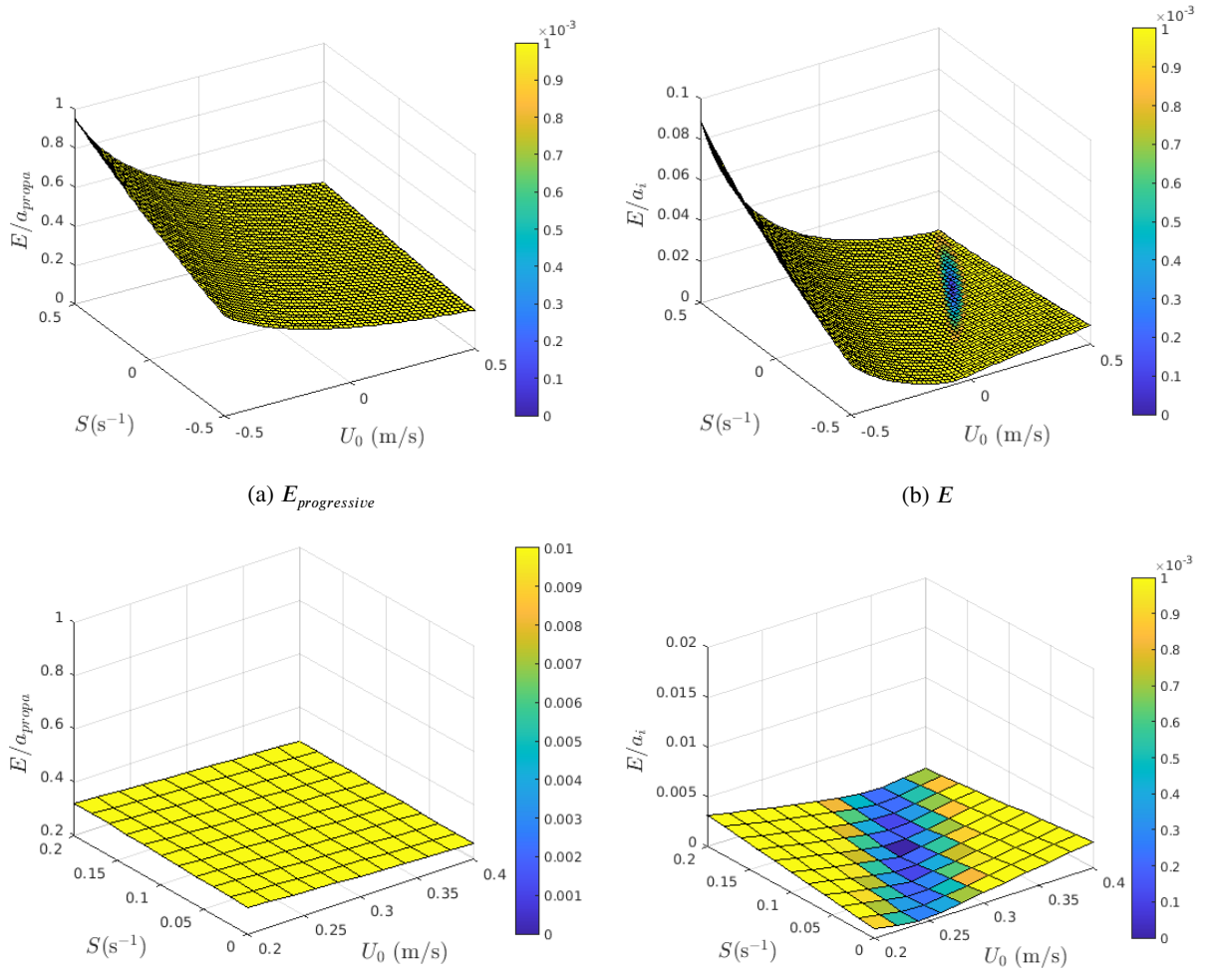

(a) $E_{progressive}$

(b) E

(c) $E_{progressive}$ zoom

(d) E zoom

Figure 8: Evolution of normalized Errors for a theoretical regular wave with reflection $R = 30$ %

$h = 1.9$ m.

We applied the algorithms for cases without current (Reg0), $U = 0$ m.s^{-1}, and in the presence of a uniform current (Reg03). Initially the nominal current sent by the pump was $U_{nom} = 0.3$ m.s^{-1} but as shown in the Fig 2 of the article by Magne et al. (2005), the current measured at the location of the four probes was $U_{measured} = 0.27$ m.s^{-1}. The periods of waves tested are in the range $T = [0.8 - 2.949]$ s and the length of the time series corresponds to the maximum number of possible periods, it is in the range $[56 - 200]$ s. An example of time series for both cases is represented in Fig. 10 (a) and (c) the signal is stationary in both conditions of current. The current intensity and the reflection obtained are represented in Fig. 10 (b) and (d). In absence of current (Fig. 10 (b)), we note that the algorithm assuming partially standing waves returns a (weak) current propagating in the opposite direction to that of the waves. However, the results remain consistent. Between 0.4 Hz and 0.6 Hz, the reflection is significant, and the algorithm assuming partially standing waves provides consistent results, whereas algorithm assuming progressive waves does not provide a good estimation of the current. In the case of regular waves in the presence of a uniform current (Fig. 10 (d)), we observe that the current recovered is on average lower than that sent by the pumps, for frequencies above 0.55 Hz the wave is progressive (low reflection), and the two algorithms give consistent results. Between 0.45 Hz and 0.55 Hz, the reflection is significant. The method assuming partially standing wave still gives a good estimate of U, contrary to the one assuming progressive wave which gives a current going in the opposite direction. Moreover, in both cases the

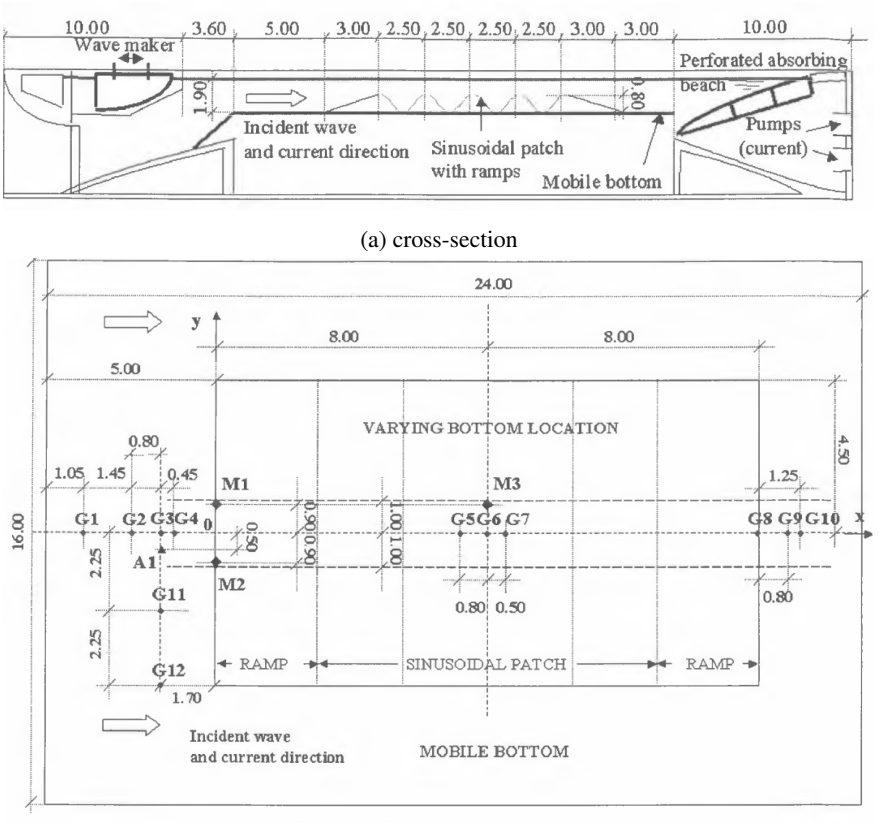

(a) cross-section

(b) Top view

Figure 9: Sketch of the experimental set-up in the BGO FIRST (Magne et al., 2005)

calculation of the wavenumber k assumes that the bottom is flat on about one wavelength. However, the presence of a sill upstream can modify the propagation conditions and the length of the flat bed is of order of the lower frequency wave-length. The discrepancies obtained may also be due to the geometry of the basin. Indeed, as demonstrated in Magne et al. (2005), the sinusoidal patch does not occupy the entire width of the basin which leads to 3D effects both on wave propagation and on the structure of the current. The presence of a Stokes drift current (Van den Bremer and Breivik, 2018) may also explain the discrepancies observed. The reflection found is the same as that in Magne et al. (2005), it is found to slowly vary with the current.

3.1.2. Opposing current

In this section the minimization method is applied using the data set from the experiment described in Laffitte et al. (2021) and presented in Fig. 11 (a). Experiments have been carried out in a wave-current flume 10 m long, 0.3 m wide and 0.5 m high (SeaTech, University of Toulon, France). The current is injected in the channel by a hydraulic pump, of maximum flow rate $Q = 0.027$ m^3 s^{-1} and measured by velocimeters. At the downstream end of the channel, a piston-type wavemaker generates regular waves in the range $[0.5 - 3.5]$ Hz by horizontal motions. The current profile is controlled by an inclined S-shape grid over the entire water column. The purpose of the experiment was to study the wave scattering by a sinusoidal bed in the presence of a vertically sheared current. In this experiment, the regular waves and the current propagate in opposite directions, with a linear vertical sheared current. All time series have a duration of 78.122 s and their frequencies are in the range $f = [0.8961 - 1.6641]$ Hz. An example of a time series for the gauge G1 is shown in Fig. 11 (b). The wave signal is found quasi-stationary in these conditions of opposite current although non-stationary turbulent conditions have been observed in large scale facility previous studies for significant opposing wave-current conditions (Draycott et al., 2019), dealing to less accurate current estimates in these configurations. A first approach is to use the method assuming a uniform current on the three probes upstream (G4, G5, G6) at the

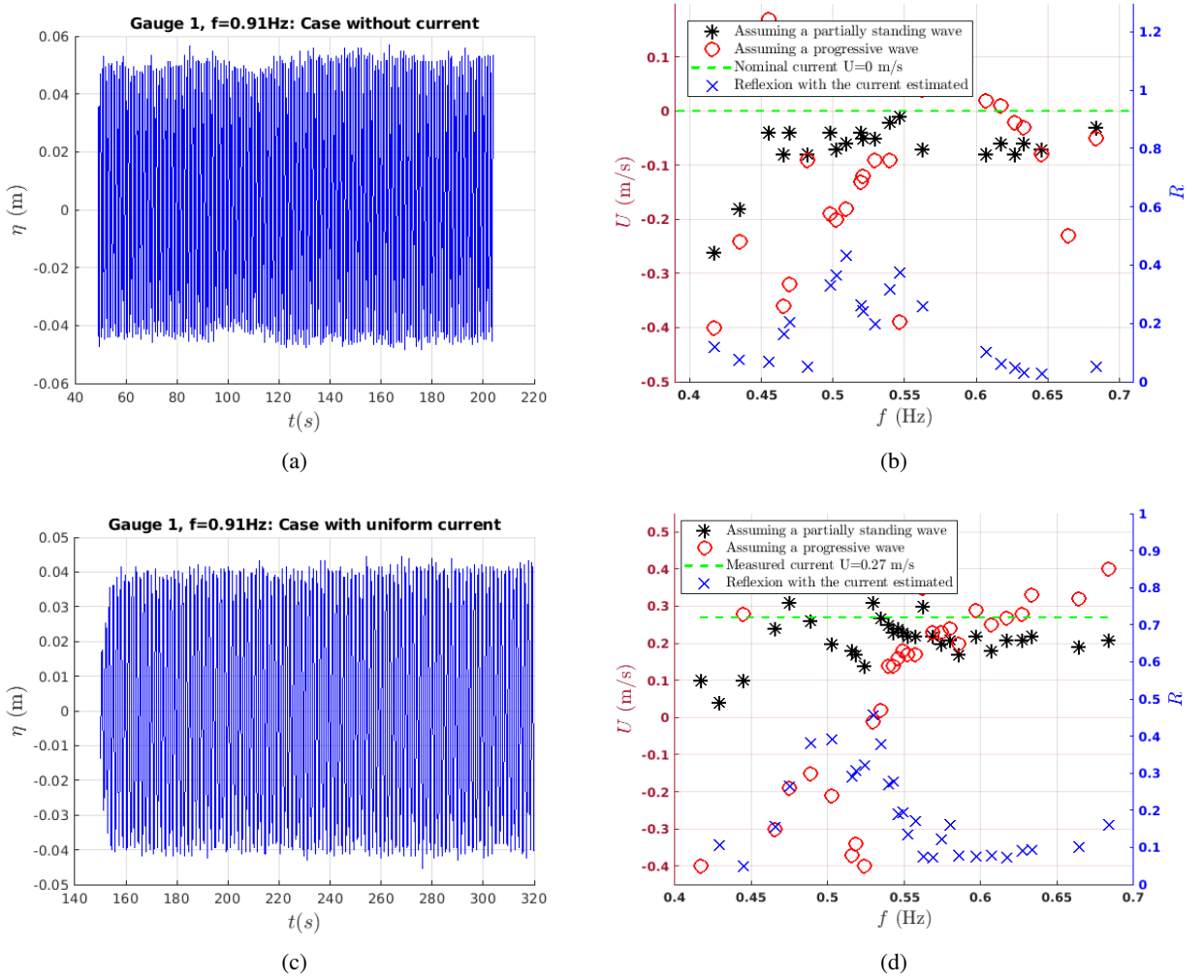

Figure 10: Section of time series for the probe G1 for the regular wave $f = 0.91$ Hz (a) without current and (c) with a uniform current. Estimated Current and Reflection for regular waves in the BGO (b) without current and (d) with a uniform current. (*)Current estimated through the algorithm assuming partially standing wave; (o) Current estimated through the algorithm assuming progressive wave; (- -) Measured current. (×) Reflection Coefficient

locations $x = 7.35; 7.65; 7.85$ m and the three probes downstream (G1, G2, G3) at the location $x = 0.75; 1.05; 1.25$ m. The water depth was $h = 0.22$ m. The current and the reflection estimated are presented in Fig. 12. For both upstream and downstream conditions, the surface current and the reflection found by Laffitte et al. (2021) have been successfully recovered using the method of minimization. The vertically averaged mean of the horizontal current measurements found by Laffitte et al. (2021) was $U_{mean} = -0.161$ m.s^{-1}. Downstream the surface current measured was $U_0 = -0.1425$ m.s^{-1}. The vertical current profile of the downstream zone is represented in the Fig 4 (a) of the article by Laffitte et al. (2021). This profile fits the results obtained by the minimization method (see (*) in Fig. 12 (a)). It's worth nothing that when reflection becomes more important (40 %), the algorithm that assumes progressive waves is no longer valid. According to Laffitte et al. (2021) at this position the current is homogeneous along the water column. Upstream, the wave reflection is weak, the near surface current measured by Laffitte et al. (2021) was $U_0 = -0.185$ m.s^{-1} which matches with the current estimated by the algorithm especially the one assuming progressive waves. At this location the current is supposed to be linear along the vertical axis. We noticed a slight variation of the current versus the frequency that could imply the presence of a linear shear. According to the theory, the uniform current assumption gives us an estimate of the current at the depth d_e: $U(-d_e) = U_0 - d_e S$, with $d_e = tanh(k^{\pm}h)/2k^{\pm}$ (Touboul et al.,

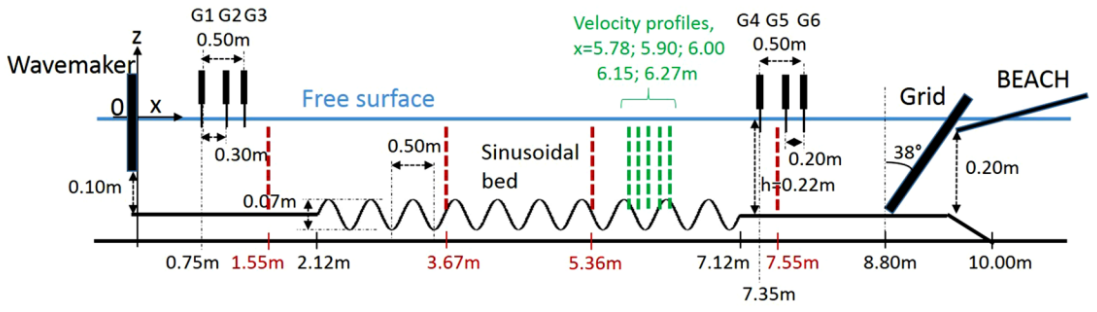

(a)

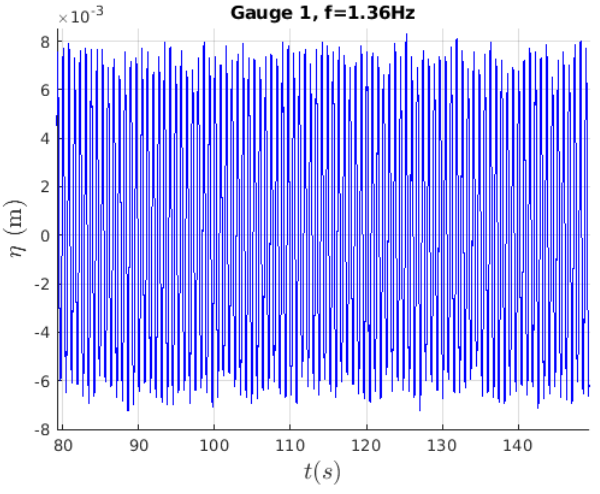

(b)

Figure 11: (a) Sketch of the experimental set-up in the wave flume (Laffitte et al., 2021). (b) Section of the time series for the probe G1 for the regular wave $f = 1.36$ Hz

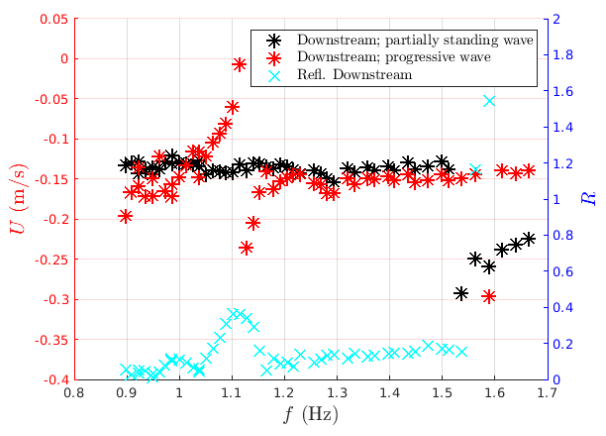

(a) Results for probes G1; G2 and G3

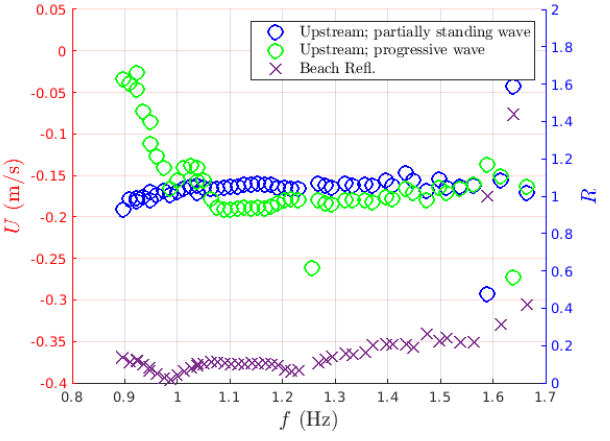

(b) Results for probes G4; G5 and G6

Figure 12: Current estimated downstream (a) ((*) red and black), Current estimated upstream (b) ((o) blue and green), Reflection ((×) cyan and violet)

2016). Since the reflection (around 10 %) is low and this current seems to be a linear function of the depth d_e, we can fit the current obtained from the algorithm assuming partially standing waves to $-d_e(k^-)$. This enables us to estimate the shear parameter S and the surface current U_0. The results are compared with the experimental measures in Fig. 13. Using this method the surface current calculated is $U_0 = -0.1503$ m.s^{-1} and the shear parameter $S = -0.269$

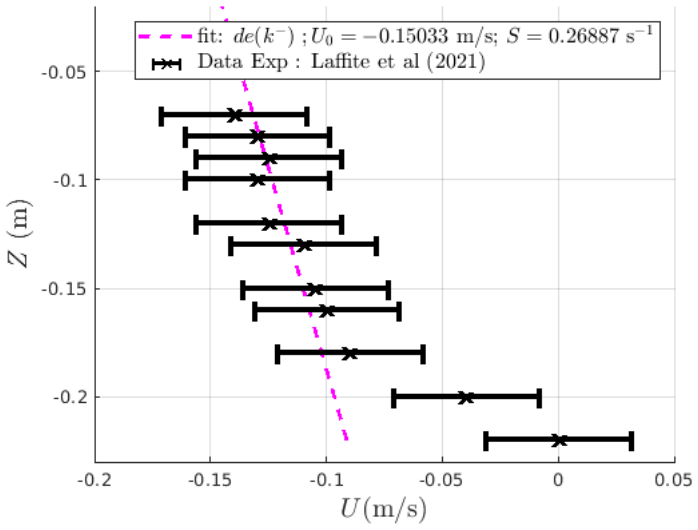

Figure 13: Current profile estimated compared to the experimental measures and the mean standard deviation

s^{-1}. It can be seen that the estimate is in agreement with the majority of the experimental points. However it does not recover the points near the bottom. There are discrepancies with the estimated values from the velocimeters presented in Laffitte et al. (2021) where $U_0 = -0.2085$ m.s^{-1} for the surface current and $S = -0.4283$ s^{-1}. This may be due to the fact that the current characteristics found by our method come from wave data whereas the experimental data points are obtained using sensors, which implies that they may be subject to measurement noise inherent to these devices. We also applied the minimization method with respect to both U_0 and S (see Fig. 14), and although we managed to recover the surface current, the impact of shear is hidden by the experimental errors, since it has less effect on wave celerity than the effect of the mean current.

3.2. Irregular waves

During the experiment in the BGO-FIRST (see the sketch of the experimental set-up in Fig. 9), the propagation of irregular waves without current and in the presence of a uniform current has also been studied. Three irregular waves spectra were generated of Jonswap type. The different parameters are presented in the following Tab. 4:

Table 4
Irregular waves parameters BGO

Case	f_p (Hz)	H_s (m)	γ	U (m.s^{-1})	Duration (s)
IR1	0.77	0.13	3.3	0	407
IR2	0.55	0.12	3.3	0	353
IR3	0.49	0.12	3.3	0	411
IR4	0.77	0.11	3.3	0.3	337
IR5	0.55	0.10	3.3	0.3	283
IR6	0.49	0.10	3.3	0.3	341

The algorithm is then applied to each component for each spectrum between $f_p/2$ and $2f_p$ and using the same four probes than in the subsection **3.1.1**. The minimization method is used first to display the smoothed spectra of the incident wave and the reflected wave, and to compare them with that of probe 1. These spectra were obtained by a

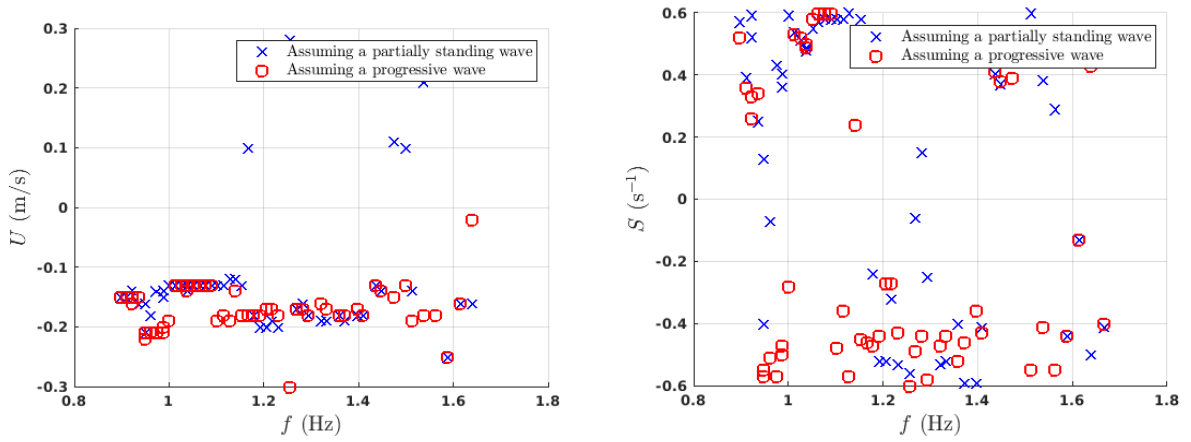

(a) Surface current estimated for each regular waves

(b) Shear parameter estimated for each regular waves

Figure 14: Surface current (a) and Shear (b) estimated by minimizing the Errors with respect to both U_0 and S. (×) Algorithm assuming partially standing waves; (o) Algorithm assuming progressive waves

moving average with a window of 21 points. The average used in this way is used to obtain the continuous (smoothed) limit of the spectrum, from the 'noisy' estimator obtained from the FFT (see Drevard et al. (2009)). An example of the spectrum and the corresponding time series for the case without current are shown in Fig.15. The estimated currents for the three sea states after the same moving window as for the wave spectra, are represented in Fig. 16. In presence of current, the spectrum and the time series are represented in Fig. 17 and the currents are represented in Fig. 18. The results shown are from the same moving window used for the spectra.

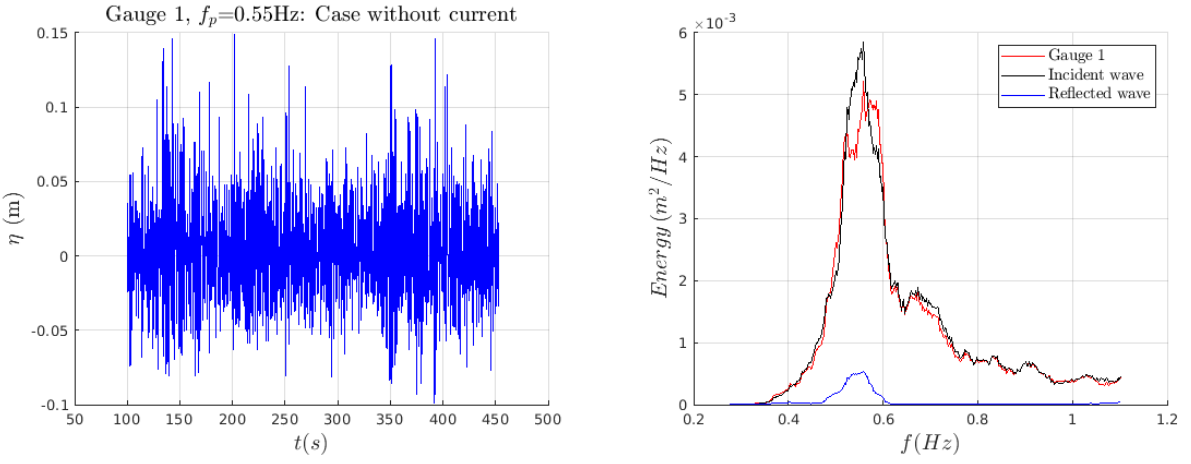

(a)

(b)

Figure 15: (a) Time series for the probe G1 of the irregular wave f_p = 0.55 Hz in the absence of current, case IR2. (b) Smoothed spectrum of the irregular wave f_p = 0.55 Hz. (-) Spectra of the probe G1; (-) Incident wave spectrum; (-)Reflected wave spectrum

Observing the spectra in both cases (Fig. 15(b) and 17(b)), we can see that the spectrum of the incident wave corresponds almost perfectly to that measured by probe 1. The differences observed can be explained by the fact that around f = 0.55 Hz the reflection becomes significant making the spectrum of the incident wave slightly different than that measured due to the combined effects of the reflected wave amplitude and of the frequency-dependent phase difference between the incident and reflected waves. In Fig. 16 and Fig. 18, case (a) corresponds to small reflected wave in the vicinity of the wave frequency peak, whereas cases (b) and (c) correspond to the highly reflected waves in

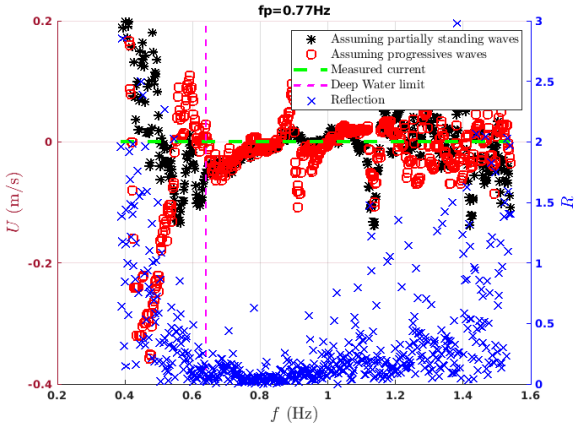

(a) Case IR1

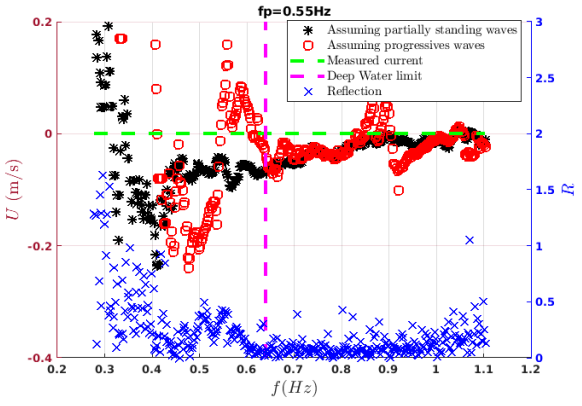

(b) Case IR2

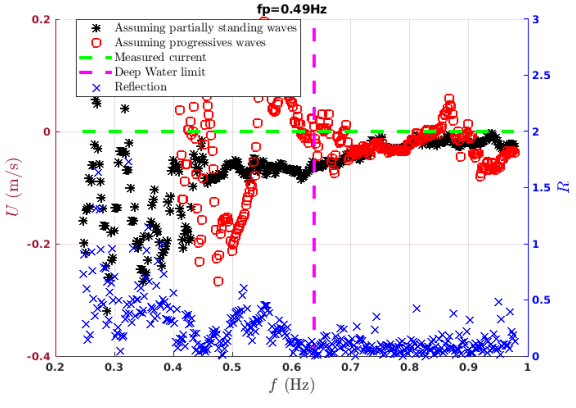

(c) Case IR3

Figure 16: Current and Reflection estimated between $f_p/2$ and $2f_p$ for irregular waves in the BGO without current. (*)Current estimated through the algorithm assuming partially standing wave; (o) Current estimated through the algorithm assuming progressive wave; (- -) Measured current. (×) Reflection Coefficient

the vicinity of the peak. In both cases we still observe that the algorithm assuming progressive waves is no longer valid when the reflection becomes significant. En particular for the two peak frequencies $f_p = 0.55$ Hz and $f_p = 0.49$ Hz. In the low frequency range (approximately between 0.2 Hz and 0.7 Hz) most of the values obtained by the algorithm assuming partially standing waves are lower than the nominal current measured in the basin. As explained in section **2.2** these discrepancies at low frequency can be due to numerical errors, by the fact that the current effect on the wavenumbers is weaker and the wavelength of the order or longer than the flat bed. At very high frequency ($f \geq 1.1$ Hz), the wave celerity against current tends to diminish (until the wave is blocked). As before, the discrepancies can also be caused by re-circulation due to the particular geometry of the basin or by the presence of a Stokes drift current. For high frequencies (0.8 Hz $\leq f \leq$ 1.1 Hz) and if the reflection is low, the current estimated by the two algorithms tends towards the expected value. At very high frequencies ($f \geq 1.1$ Hz), the differences may be due to the divergence of the coefficient s_5.

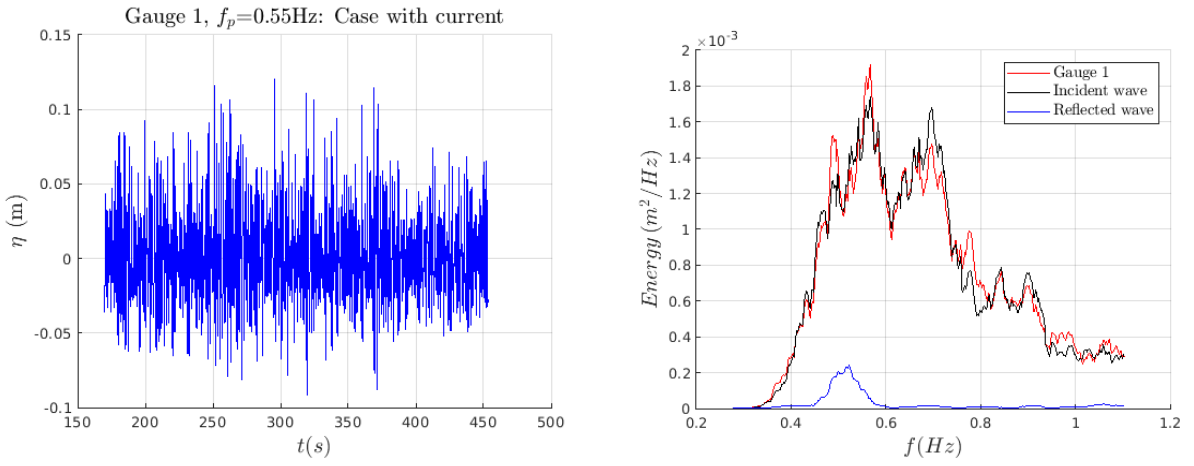

(a) (b)

Figure 17: (a) Time series for the probe G1 of the irregular wave f_p = 0.55 Hz in the presence of current, case IR5. (b) Smoothed spectrum of the irregular wave f_p = 0.55 Hz. (-) Spectra of the probe G1; (-) Incident wave spectrum; (-)Reflected wave spectrum

4. Discussion

The use of the minimization methods on data from basin or canal experiments has allowed us to verify their applicability for the calculation of the current intensity and structure, for either following or opposing current conditions. The use of algorithms that do and do not take into account the presence of a reflected wave has enabled us to study the sensitivity of the current calculation to the presence of such wave conditions. Concerning the vertical structure of the current, a direct minimisation of the error with respect to both surface current and shear, assumed constant, was first carried out. Knowing that wave speed is influenced by the current over a depth that is all the greater the lower its frequency, a second method was proposed, first by calculating the average current seen by the wave, then, taking advantage of the knowledge of this value as a function of frequency, to calculate the shear, assumed to be constant.

The analyses involved data from regular waves, over a wide frequency range, and irregular waves, with Jonswap-type spectra. For irregular waves, frequency averaging was used to estimate continuous spectra, based on discrete FFT calculations of the wave's incident and reflected components. The same frequency averaging was used to calculate the current, thus obtained over the frequency range $[f_{pic}/2; 2f_{pic}]$. Vertical shear current conditions have been studied for opposing wave current conditions.

For progressive waves in the presence of homogeneous current, we observed that either for following or opposing current conditions, methods assuming progressive or partially standing waves give similar results in quite good agreement between the measured and the calculated current. However, the values observed are slightly lower than those expected for the experiments for both regular and irregular waves of Magne et al. (2005). A similar observation can be made for low frequencies in the case of irregular waves. On the other hand, at high frequencies, the current obtained tends towards the expected value. For partially standing waves, the method based on progressive waves falls even for relative small reflection (about 20 % in amplitude, few percents in terms of wave energy or wave action). That means that wave reflection must be taken into account when two wave fields propagate in opposing directions.

For vertically shear currents, considered in the experiments of Laffitte et al. (2021) in opposing wave current conditions, we observed that a direct minimisation with respect to both surface current and shear did not allow to estimate de shear. This was ascribed to the fact that for moderate shears, effect of the shear on the wave velocity is much smaller that the effect of the current. On the contrary, the calculated current appeared much less noisy (see Fig. 14). By proceeding in two stages, with a first calculation of the averaged current, we were able to access the shear from the data of the average current obtained as a function of frequency. Although the results are satisfactory, the method is based on the assumption of linear waves and non-turbulent flow. Non-linear effects can influence the results obtained, such as the presence of a Stokes drift current. Stokes drift describes the difference between the wave-averaged velocity

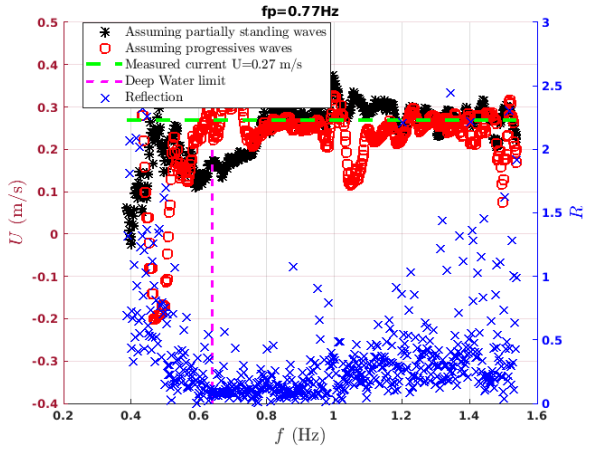

(a) Case IR4

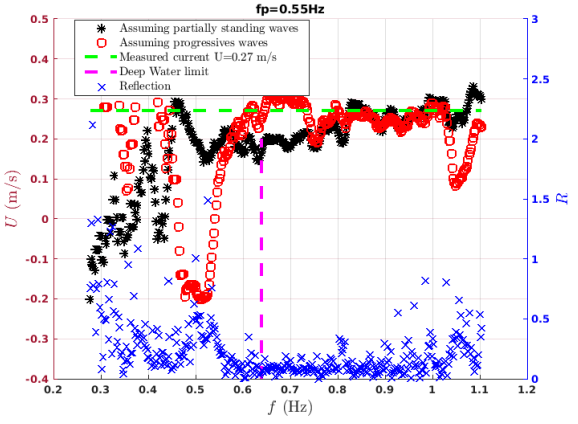

(b) Case IR5

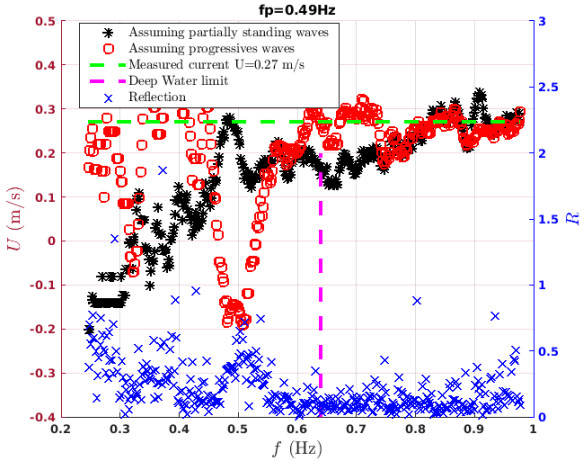

(c) Case IR6

Figure 18: Current and Reflection estimated between $f_p/2$ and $2f_p$ for irregular waves in the BGO in the presence of a uniform current. (*)Current estimated through the algorithm assuming partially standing wave; (o) Current estimated through the algorithm assuming progressive wave; (- -) Measured current. (×) Reflection Coefficient

experienced by a moving particle (from a Lagrangian viewpoint) and the velocity observed in a stationary reference frame (from an Eulerian viewpoint) (Stokes, 1847). In deep water it is defined as follows:

$$u_{SD}(z) = c(ak)^2 e^{2kz} + O((ak)^6) \tag{13}$$

Ursell (1953) extended this relationship to finite depth:

$$u_{SD}(z) = c(ak)^2 \frac{cosh(2k(h+z))}{2(sinh^2((kh)))} \tag{14}$$

where c is the wave celerity, ak the wave curvature, k the wave number and h the water depth. We applied these equations to the regular waves, propagating without current, from the BGO experiment (case Reg0). The Fig. 19 represents the stokes drift current at the surface and the mean stokes drift current obtained according to the frequency. The mean Stokes drift current was obtained by integrating Eq. (13) and (14) over half a wavelength with respect to z for deep water depth, and over the water column for finite water depth. On average we find a stokes drift current around 1 cm.s^{-1}. This can partially explains the fact that a weak current is found when it is supposed to be absent. The

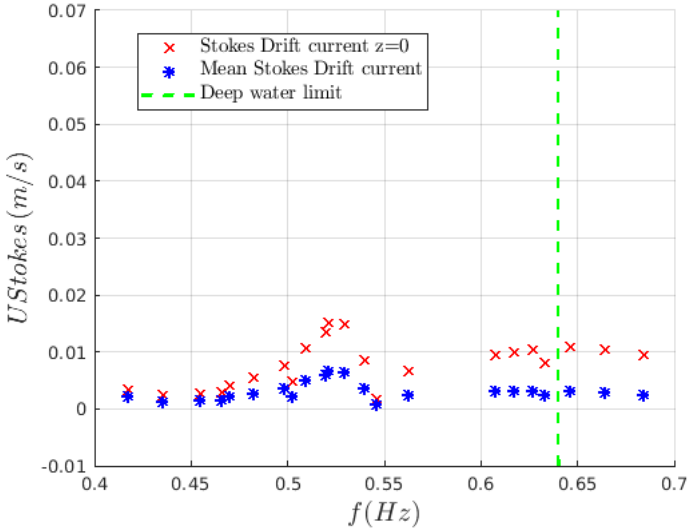

Figure 19: Stokes drift current calculated through the data from the case of regular waves without current at the BGO. (*) Mean Stokes drift current. (×) Stokes drift current at the surface.

discrepancies observed, in the BGO, can be also due to to the geometry of the basin and the slope of the bottom. Indeed, we made the assumption of a homogeneous environment but in reality 3D effects may arise because the sinusoidal bottom does not cover the entire width of the pool. This non-uniform distribution of momentum induces re-circulation within the basin. This last assumption must be taken into account for both regular and irregular waves for the experiments carried out in the BGO First basin. As mention by Draycott et al. (2019), non-stationary turbulent conditions are observed for opposing wave current conditions, that alters the quality of the results. In the experiments of Laffitte et al. (2021), only carried out for regular waves, we did not observe such an effect on the quality of the results concerning the calculation of the current intensity and shear. However, the flow is rotational and evolves in the direction of wave propagation, as shown by the shear evolution between the upstream and downstream probe positions.

5. Conclusion

Decades ago, research on currents influencing wave propagation velocity was limited to models assuming uniform currents. This study takes advantage of a minimization method for estimating current shape in the water column and intensity from wave data, with promising theoretical results applicable to both monochromatic and real waves including partially standing waves. In the experimental settings, the minimization method was used to retrieve surface current intensity and the shear from regular and irregular wave measurements. Since the effect of shear on wave velocity is often much smaller than that of average current, the calculation of current as a function of frequency becomes necessary, not only for a better estimate of current by a possibly weighted average over frequencies, but also out of necessity for the calculation of shear, assumed in this study to be constant. In the present, we restricted ourselves to the 2D case of partially standing waves, but the method can be extended to the 3D case by taking account of waves propagating in different directions. In the simplest case of two wave fields propagating in opposing directions, the above method can be applied with the use of oversampled system of gauges displayed in the horizontal plane, and by a minimisation of the error with respect to both current intensity and direction, the direction being that of the two waves. Note that in this particular case, only the current component in the direction of the waves can be recovered, as is the case with HF radar techniques where surface current measurements are recovered in the direction of the electromagnetic wave. For a full calculation of the current, at least two non-opposed directions of wave propagation are necessary. Calculations are in progress for partially oblique reflected waves from data collected during a campaign carried out recently at the BGO FIRST as part of the ANR project MORHOC'H 2. The method may also be applicable to wave spectra with angular distribution, as studied by Pillai et al. (2021) to extract the current intensity from buoy data.

Acknowledgment

The AID (French Defence Innovation Agency) is acknowledged for funding the PhD grant of A.Cuevas, as well as the ANR maturation MORHOC'H 2.

References

Belibassakis, K., Touboul, J., Laffitte, E., Rey, V., 2019. A mild-slope system for bragg scattering of water waves by sinusoidal bathymetry in the presence of vertically sheared currents. Journal of Marine Science and Engineering 7, 9. doi:https://doi.org/10.3390/jmse7010009.

Van den Bremer, T.S., Breivik, Ø., 2018. Stokes drift. Philosophical Transactions of the Royal Society A: Mathematical, Physical and Engineering Sciences 376, 20170104.

Draycott, S., Pillai, A., Ingram, D., Johanning, L., 2019. Resolving combined wave-current fields from measurements using interior point optimization. Coastal Engineering 149, 4–14.

Draycott, S., Steynor, J., Davey, T., Ingram, D.M., 2018. Isolating incident and reflected wave spectra in the presence of current. Coastal Engineering Journal 60, 39–50.

Drevard, D., Rey, V., Fraunié, P., 2009. Partially standing wave measurement in the presence of steady current by use of coincident velocity and/or pressure data. Coastal engineering 56, 992–1001. doi:https://doi.org/10.1016/j.coastaleng.2009.06.002.

Haas, K.A., Svendsen, I.A., 2002. Laboratory measurements of the vertical structure of rip currents. Journal of geophysical research: oceans 107, 15–1. doi:10.1029/2001JC000911.

Kirby, J.T., Chen, T.M., 1989. Surface waves on vertically sheared flows: approximate dispersion relations. Journal of Geophysical Research: Oceans 94, 1013–1027.

Laffitte, E., Rey, V., Touboul, J., Belibassakis, K., 2021. Water wave scattering by a sinusoidal bed in the presence of vertically sheared current. Applied Ocean Research 108, 102549. doi:https://doi.org/10.1016/j.apor.2021.102549.

Magne, R., Rey, V., Ardhuin, F., 2005. Measurement of wave scattering by topography in the presence of currents. Physics of Fluids 17. doi:https://doi.org/10.1063/1.2140283.

Mansard, E.P., Funke, E., 1980. The measurement of incident and reflected spectra using a least squares method, in: Coastal Engineering 1980, pp. 154–172. doi:https://doi.org/10.1061/9780872622647.008.

Pillai, A.C., Davey, T., Draycott, S., 2021. A framework for processing wave buoy measurements in the presence of current. Applied Ocean Research 106, 102420.

Rey, V., Capobianco, R., Dulou, C., 2002. Wave scattering by a submerged plate in presence of a steady uniform current. Coastal Engineering 47, 27–34. doi:https://doi.org/10.1016/S0378-3839(02)00096-0.

Rey, V., Charland, J., Touboul, J., 2014. Wave–current interaction in the presence of a three-dimensional bathymetry: Deep water wave focusing in opposing current conditions. Physics of Fluids 26. doi:https://doi.org/10.1063/1.4894740.

Smeltzer, B.K., Æsøy, E., Ådnøy, A., Ellingsen, S.Å., 2019. An improved method for determining near-surface currents from wave dispersion measurements. Journal of Geophysical Research: Oceans 124, 8832–8851.

Soulsby, R., 1990. Tidal current boundary layers, the sea, part 1. Edited by: B. Le Méhauté, University of Miami, USA, John Wiley & Sons Inc., Printed in USA, ISBN: 0 471 63393 3 .

Stewart, R.H., Joy, J.W., 1974. Hf radio measurements of surface currents, in: Deep sea research and oceanographic abstracts, Elsevier. pp. 1039–1049.

Stokes, G.G., 1847. On the theory of oscillatory waves. Transactions of the Cambridge Philosophical Society 8, 441–455.

Tabeshpour, M.R., Belvasi, N., 2023. Ocean waves time-series generation: minimum required artificial wave time-series for wave energy converter analysis. Journal of Marine Engineering & Technology , 1–11doi:https://doi.org/10.1080/20464177.2023.2197280.

Touboul, J., Belibassakis, K., 2019. A novel method for water waves propagating in the presence of vortical mean flows over variable bathymetry. Journal of Ocean Engineering and Marine Energy 5, 333–350.

Touboul, J., Charland, J., Rey, V., Belibassakis, K., 2016. Extended mild-slope equation for surface waves interacting with a vertically sheared current. Coastal Engineering 116, 77–88. doi:https://doi.org/10.1016/j.coastaleng.2016.06.003.

Ursell, F., 1953. The long-wave paradox in the theory of gravity waves, in: Mathematical Proceedings of the Cambridge Philosophical Society, Cambridge University Press. pp. 685–694.

Yurovskaya, M., Kudryavtsev, V., Chapron, B., Collard, F., 2019. Ocean surface current retrieval from space: The sentinel-2 multispectral capabilities. Remote sensing of Environment 234, 111468. doi:https://doi.org/10.1016/j.rse.2019.111468.